



Defense Threat Reduction Agency  
8725 John J. Kingman Road, MS 6201  
Fort Belvoir, VA 22060-6201



DTRA-TR-13-64

**TECHNICAL REPORT**

# Nanowires for THz Spectroscopy

Approved for public release; distribution is unlimited.

October 2013

HDTRA1-03-D-0009

Mansoor Sheik-Bahae

Prepared by:  
OVPR/ University Strategic  
Partnership  
MSC02 1660  
1 University of New Mexico  
Albuquerque, New Mexico 87131

**DESTRUCTION NOTICE:**

Destroy this report when it is no longer needed.  
Do not return to sender.

PLEASE NOTIFY THE DEFENSE THREAT REDUCTION  
AGENCY, ATTN: DTRIAC/ J9STT, 8725 JOHN J. KINGMAN ROAD,  
MS-6201, FT BELVOIR, VA 22060-6201, IF YOUR ADDRESS  
IS INCORRECT, IF YOU WISH THAT IT BE DELETED FROM THE  
DISTRIBUTION LIST, OR IF THE ADDRESSEE IS NO  
LONGER EMPLOYED BY YOUR ORGANIZATION.

# REPORT DOCUMENTATION PAGE

Form Approved  
OMB No. 0704-0188

Public reporting burden for this collection of information is estimated to average 1 hour per response, including the time for reviewing instructions, searching existing data sources, gathering and maintaining the data needed, and completing and reviewing this collection of information. Send comments regarding this burden estimate or any other aspect of this collection of information, including suggestions for reducing this burden to Department of Defense, Washington Headquarters Services, Directorate for Information Operations and Reports (0704-0188), 1215 Jefferson Davis Highway, Suite 1204, Arlington, VA 22202-4302. Respondents should be aware that notwithstanding any other provision of law, no person shall be subject to any penalty for failing to comply with a collection of information if it does not display a currently valid OMB control number. **PLEASE DO NOT RETURN YOUR FORM TO THE ABOVE ADDRESS.**

<b>1. REPORT DATE (DD-MM-YYYY)</b> 00-10-2013		<b>2. REPORT TYPE</b> Technical		<b>3. DATES COVERED (From - To)</b> 07/21/2010 - 04/30/2012	
<b>4. TITLE AND SUBTITLE</b> Nanowires for THz Spectroscopy				<b>5a. CONTRACT NUMBER</b> HDTRA1-03-D-0009	
				<b>5b. GRANT NUMBER</b>	
				<b>5c. PROGRAM ELEMENT NUMBER</b>	
<b>6. AUTHOR(S)</b> Mansoor Sheik-Bahae				<b>5d. PROJECT NUMBER</b> 3	
				<b>5e. TASK NUMBER</b> 26	
				<b>5f. WORK UNIT NUMBER</b>	
<b>7. PERFORMING ORGANIZATION NAME(S) AND ADDRESS(ES)</b> OVPR/University Strategic Partnership MSC02 1660 1 University of New Mexico Albuquerque, NM 87131				<b>8. PERFORMING ORGANIZATION REPORT NUMBER</b> OVPRED 798B	
<b>9. SPONSORING / MONITORING AGENCY NAME(S) AND ADDRESS(ES)</b> Defense Threat Reduction Agency 8725 John J. Kingman Road STOP 6201 Fort Belvoir, VA 22060 PM/James Reed				<b>10. SPONSOR/MONITOR'S ACRONYM(S)</b> DTRA	
				<b>11. SPONSOR/MONITOR'S REPORT NUMBER(S)</b> DTRA-TR-13-64	
<b>12. DISTRIBUTION / AVAILABILITY STATEMENT</b> Approved for public release; distribution is unlimited.					
<b>13. SUPPLEMENTARY NOTES</b>					
<b>14. ABSTRACT</b> Detailed experimental investigation of THz emission mechanisms in InAs nanowires is performed. Multiple independent measurements are brought into quantitative agreement by means of the developed model, which includes contributions of quantized surface plasmon modes of the cylindrical nanowire geometry. THz emission from ordered array of InAs nanowires is also investigated, and model predictions are verified using developed broadband THz spectrometer. Novel pyramid hexagonal lattice structures developed during this work have proven as extremely broadband (octave-spanning) THz nanoscale emitter sources with attractive potential for a variety of applications. To perform broadband measurements, novel THz spectrometer has been developed with operating up to 20 THz. Novel electro-absorption sampling technique has been developed using multiple quantum well structures. Franz-Keldysh effect has been identified as the main detection mechanism and coherent detection of THz pulses has been demonstrated. THz imaging with electro-absorption effect using conventional (visible wavelengths) imaging systems has also been demonstrated.					
<b>15. SUBJECT TERMS</b> Ultrafast THz spectroscopy, THz nanowire emitters, THz imaging, nanowire detection, InAs nanowires					
<b>16. SECURITY CLASSIFICATION OF:</b>			<b>17. LIMITATION OF ABSTRACT</b> UU	<b>18. NUMBER OF PAGES</b> 20	<b>19a. NAME OF RESPONSIBLE PERSON</b> James Reed
<b>a. REPORT</b> Unclassified	<b>b. ABSTRACT</b> Unclassified	<b>c. THIS PAGE</b> Unclassified			<b>19b. TELEPHONE NUMBER (include area code)</b> 703-767-8793

## CONVERSION TABLE

Conversion Factors for U.S. Customary to metric (SI) units of measurement.

MULTIPLY  $\longrightarrow$  BY  $\longrightarrow$  TO GET  
 TO GET  $\longleftarrow$  BY  $\longleftarrow$  DIVIDE

angstrom	1.000 000 x E -10	meters (m)
atmosphere (normal)	1.013 25 x E +2	kilo pascal (kPa)
bar	1.000 000 x E +2	kilo pascal (kPa)
barn	1.000 000 x E -28	meter <sup>2</sup> (m <sup>2</sup> )
British thermal unit (thermochemical)	1.054 350 x E +3	joule (J)
calorie (thermochemical)	4.184 000	joule (J)
cal (thermochemical/cm <sup>2</sup> )	4.184 000 x E -2	mega joule/m <sup>2</sup> (MJ/m <sup>2</sup> )
curie	3.700 000 x E +1	*giga bacquerel (GBq)
degree (angle)	1.745 329 x E -2	radian (rad)
degree Fahrenheit	$t_k = (t^{\circ}f + 459.67)/1.8$	degree kelvin (K)
electron volt	1.602 19 x E -19	joule (J)
erg	1.000 000 x E -7	joule (J)
erg/second	1.000 000 x E -7	watt (W)
foot	3.048 000 x E -1	meter (m)
foot-pound-force	1.355 818	joule (J)
gallon (U.S. liquid)	3.785 412 x E -3	meter <sup>3</sup> (m <sup>3</sup> )
inch	2.540 000 x E -2	meter (m)
jerk	1.000 000 x E +9	joule (J)
joule/kilogram (J/kg) radiation dose absorbed	1.000 000	Gray (Gy)
kilotons	4.183	terajoules
kip (1000 lbf)	4.448 222 x E +3	newton (N)
kip/inch <sup>2</sup> (ksi)	6.894 757 x E +3	kilo pascal (kPa)
ktap	1.000 000 x E +2	newton-second/m <sup>2</sup> (N-s/m <sup>2</sup> )
micron	1.000 000 x E -6	meter (m)
mil	2.540 000 x E -5	meter (m)
mile (international)	1.609 344 x E +3	meter (m)
ounce	2.834 952 x E -2	kilogram (kg)
pound-force (lbs avoirdupois)	4.448 222	newton (N)
pound-force inch	1.129 848 x E -1	newton-meter (N-m)
pound-force/inch	1.751 268 x E +2	newton/meter (N/m)
pound-force/foot <sup>2</sup>	4.788 026 x E -2	kilo pascal (kPa)
pound-force/inch <sup>2</sup> (psi)	6.894 757	kilo pascal (kPa)
pound-mass (lbm avoirdupois)	4.535 924 x E -1	kilogram (kg)
pound-mass-foot <sup>2</sup> (moment of inertia)	4.214 011 x E -2	kilogram-meter <sup>2</sup> (kg-m <sup>2</sup> )
pound-mass/foot <sup>3</sup>	1.601 846 x E +1	kilogram-meter <sup>3</sup> (kg/m <sup>3</sup> )
rad (radiation dose absorbed)	1.000 000 x E -2	**Gray (Gy)
roentgen	2.579 760 x E -4	coulomb/kilogram (C/kg)
shake	1.000 000 x E -8	second (s)
slug	1.459 390 x E +1	kilogram (kg)
torr (mm Hg, 0 <sup>o</sup> C)	1.333 22 x E -1	kilo pascal (kPa)

\*The bacquerel (Bq) is the SI unit of radioactivity; 1 Bq = 1 event/s.

\*\*The Gray (GY) is the SI unit of absorbed radiation.

## TABLE OF CONTENTS:

I.	Introduction .....	01
II.	Understanding of THz emission mechanism in nanowires .....	03
III.	Development of broadband THz detection schemes	
	a) Incoherent detection .....	06
	b) Coherent detection and imaging .....	08
IV.	THz reflection and emission studies of ordered nanowires .....	10
V.	Dissemination of this work .....	13
VI.	Conclusion .....	13
	References .....	14
	Appendix A (reproduction of Nature Photonics feature article) .....	16

## I. Introduction

Control of electromagnetic fields at sub-wavelength dimensions is an emerging need for increased functionality in nanoscience and nanotechnology [1]. This is accomplished by manipulation of material properties and geometries at the nanoscale [2]. For example, the response of charge carriers to external perturbations gives rise to modified behavior of slab plasmon and plasmon–polariton modes in confined geometries [3]. The conversion of electromagnetic radiation into propagating charge carrier waves allows geometric control, localization [4], and guiding of light at subwavelength dimensions [5]. These are the examples of the advantages of the nanoscale control of light-matter interaction which has provided led to the emerging field of plasmonics or metal optics. A particularly interesting area is that of plasmonics in the terahertz (THz) regime, where, e.g., recent research on the excitation of surface plasmon modes in tapered metal wire geometries demonstrated imaging of electronic characteristics of materials on micro- and nanoscales [6].

Improvement of the time-resolved nanoscale imaging at THz frequencies requires an efficient local emitter/detector combined with broadband time-domain spectroscopy methods. Nanostructured semiconductors, in combination with recent techniques for high-power, ultrafast THz excitation sources, can serve as intense THz nanoscale emitters. Nanowires have been the subject of extensive ultrafast spectroscopic studies at visible and near infrared frequencies [7]. The emission of THz pulses has been reported from a variety of nanostructures but the nature of the ultrafast excitation mechanism is still not well understood.

In this work, we showed that InAs nanowires can serve as highly efficient radiators of THz frequency electromagnetic transients. We argued that nanowires overcome the problem of internal reflection that occurs at the air–semiconductor macroscale interface, leading to much higher emission efficiency compared to planar substrates. Analysis of the dielectric function, including transverse confinement, suggests that the emission originates from low-energy (acoustic) surface plasmon–polariton modes.

To make these studies possible, we designed and implemented a broadband THz spectrometer as well as novel THz detection and imaging schemes. Incoherent detection and novel coherent electro-absorption sampling using multiple quantum well structures have been demonstrated with bandwidth exceeding 15 THz. THz imaging has also been demonstrated using electro-absorption sampling and conventional visible imaging hardware.

Using newly developed instrumentation, we investigated THz generation mechanisms in semiconducting nanowires (NWs) and have found it to be quite different compared to well-known case of bulk semiconductors. Corroborating data with our collaborators, we came to a novel conclusion that excitation of the acoustic surface plasmon modes is responsible for the THz emission properties of the NWs. This conclusion implied high frequency of the bulk plasmon ( $> 10$  THz), the regime usually not accessible to conventional THz spectroscopy. Using our broadband spectrometer we performed THz reflection studies of the NWs and have verified the presence of high frequency bulk plasmon mode, providing further verification of our model.

We have also performed exploratory studies to investigate THz emission from ordered nanowires, fabricated by a novel approach, developed by our collaborators at Sandia National Laboratories. We identified plasmon and phonon contributions to the emitted signals. In particular, we have found that novel “pyramid” InAs structures provide extremely broadband and efficient THz emission, serving as good candidates for flexible THz sources.

Our accomplishments can be divided into three parts:

- 1) Understanding of THz emission mechanism in nanowires (Section II).
- 2) Development of broadband THz detection schemes (Section III).
- 3) THz reflection and emission studies of ordered nanowires (Section IV).

Below is a more detailed explanation of each of these advancements.

## II. Understanding of THz emission mechanism in nanowires

Based on our collaboration with Sandia National Laboratories we experimentally investigated THz emission from InAs nanowires (NWs). InAs NWs are grown by vapor-liquid-solid epitaxial technique, where tri-methyl indium and AsH<sub>3</sub> atmospheres induce self-assembly of In and As into InAs semiconducting nanowires [1]. Thus, control sample is required, as some InAs is spent in forming epilayer underneath the self-assembled NWs and hence can contribute to the THz emission signals (Figure 1).

The summary of the results is shown in Figure 2, where THz emission from InAs NWs, bulk InAs and control sample are compared. As shown, NWs emit comparable levels of THz radiation and correspond to 15-fold enhancement over the bulk semiconductor, when its surface fill factor is taken into account. This enhancement we explained by the plasma dipole orientation, more conducive for THz radiation outcoupling, as compared to the bulk. Additionally, we compared carrier density, extracted from the THz emission signal assuming bulk Drude response, with the independent transconductance measurements, performed at Sandia National Laboratories, Livermore CA [8]. A factor of 40 disagreement between transconductance and THz measurements point to the fact that bulk Drude response is not applicable in description of the longitudinal modes of the NW system.

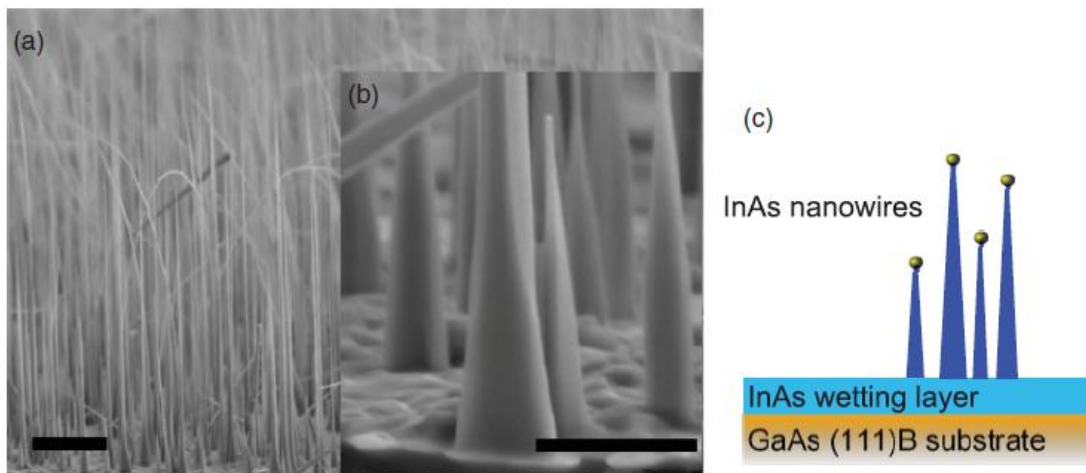


**Figure 1:** (a) Scanning electron microscope image of the InAs NW array (scale bar is 3  $\mu\text{m}$ ); (b) inset showing more detail of the individual NWs (scale bar 1  $\mu\text{m}$ ); (c) schematic representation of the NWs and the wetting layer, resulting from the VLS growth technique.

To gain a deeper understanding of the physics of carrier transport in semiconductor nanowires, we moved beyond our unbounded three dimensional model that has been used with great success to interpret earlier experiments with bulk substrates. Reduced dimensionality will have implications for charge carrier dynamic that will directly affect the radiation properties of the wires. The relevant dimensions are both wire diameter ( $\sim 100$  nm) and the wire length ( $> 1$   $\mu\text{m}$ ).

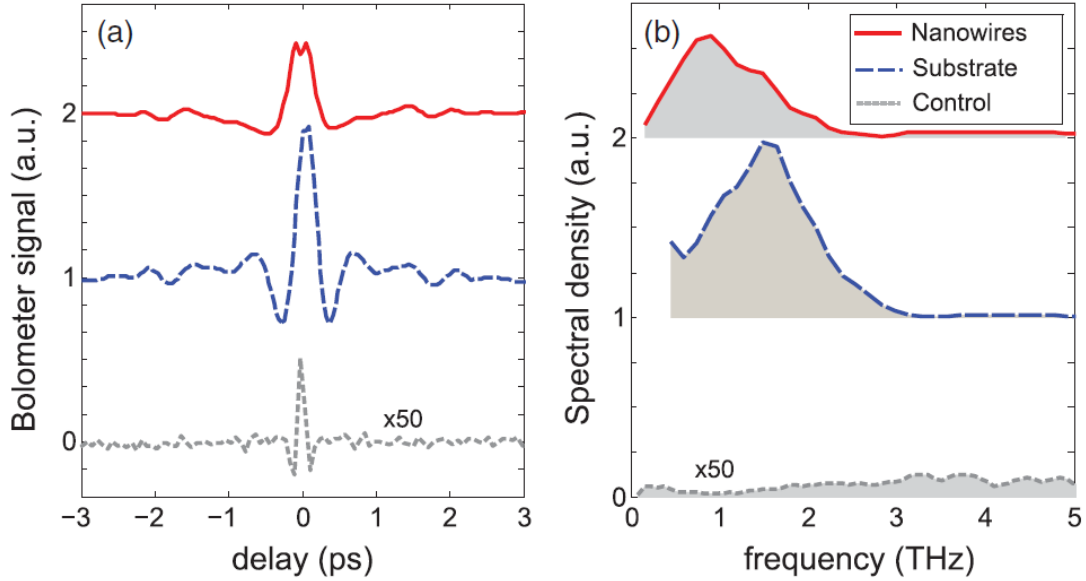


**Figure 2:** Linear autocorrelations (panel a) and corresponding linear spectrum (panel b) of the THz emission from InAs nanowires (top, red), bulk InAs substrate (middle, blue) and control (bottom, gray), as explained in the text.

It is important to point out that the small diameter of the nanowires is not causing quantum confinement of individual electron energy levels as would occur in a quantum well with a characteristic length scale of 10 nm or less. Here we are interested in plasma confinement on a dimension of  $\sim 100$  nm. This means that *collective* behavior of electrons as manifest in the plasma dynamics may be affected by the wire geometry.

We have performed modeling of dielectric function of nanowires, modifying existing models of the electron-loss spectroscopy in the presence of conducting cylinders [9]. To this end, we quantized plasmon wavevector along the length ( $L$ ) of the NW, with the mode number  $n$ , while the azimuthal component is described by the quantum number  $l$ , forming orthogonal mode set  $(n, l)$  (see Ref. 10 for more details). Figure 3 (left) shows mode profiles for fixed  $n=3$  and varying  $l$ . Dispersion of these modes can be seen in Figure 3 (right), which shows calculation of the plasmon modes in NWs, considering the effect of background dielectric constant of the semiconductor. While bulk and higher order ( $l$ ) surface plasmon modes are nearly dispersionless,  $l=0$  mode corresponds to strong (linear) dispersion for small values of the normalized wavevector (x-axis). This is the so called *acoustic plasmon* mode. The inset shows linear dispersion of the  $l=0$  mode, and a value of the normalized wavevector at 1 THz emission (Figure 2). While bulk plasmon is at 12 THz (Figure 3), consistent with the transconductance measurement, its acoustic counterpart is at the observed 1 THz frequency, bringing modeling and two independent experiments into a quantitative agreement. We note that due to inclusion of the background dielectric constant, higher order modes ( $l>0$ ) are at the 0.95 of the plasma frequency for given constants of InAs.

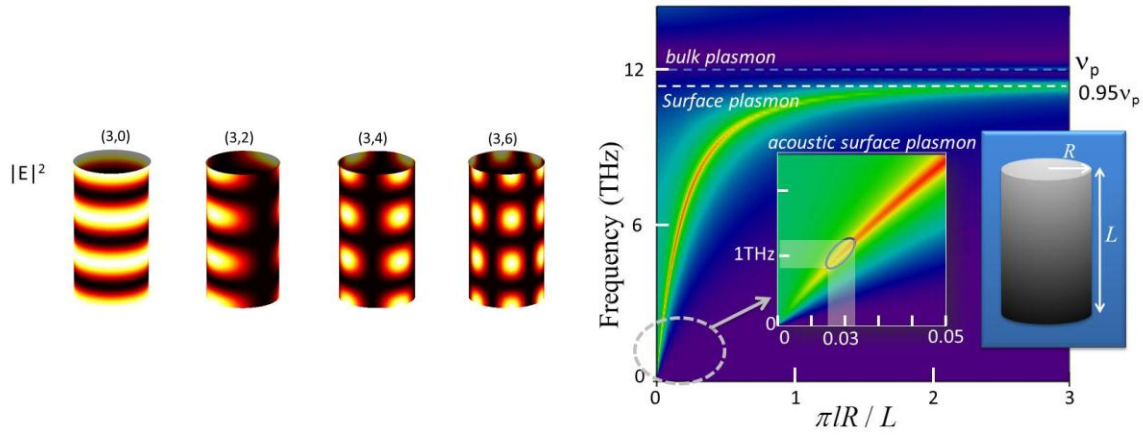


**Figure 3:** (left) Intensity pattern of the  $(n,l)$  plasmon modes in cylindrical NWs; (right) the dispersion function of the InAs nanowires, including the effects of background (optical) dielectric constant.

In addition to the modeling of the plasmon physics we have also modeled instrument response of our detection system, based on the standard implementation of the THz spectrometer [11]. This implementation is based on interference of THz emission sources, generated by identical near-infrared excitation pulses. We identified the importance of spatial interference effects in detrimentally influencing (filtering) the detected spectral characteristics of the nanowires. This is particularly important for high frequency studies, where presence of bulk plasmon modes, predicted at 12 THz for our InAs samples, can be observed.

With this in mind, we have designed and implemented our novel broadband THz spectrometer, with which both THz emission, THz reflection and transmission studies are now possible.

### III. Development of broadband THz detection schemes

Proper characterization of bulk and nano-structured semiconductors requires clear identification of their plasma edge frequencies, which may exceed 12 THz. This is well beyond the reach of THz time-domain spectroscopy based on electro-optic sampling (coherent detection) or two-pulse THz spectrometer mentioned above (incoherent detection, i.e. phase information of THz is lost, only linear spectral information is available).

The need for broadband spectroscopy of the condensed resonances has motivated our development of a broadband THz Fourier transform spectrometer with bandwidth of 15 THz or greater. We designed and implemented our broadband THz spectrometer with both coherent and incoherent detection schemes.

#### a) Incoherent detection:

Schematic of our incoherent detection scheme is shown in Figure 4. We solve the problem of spatial filtering in a two-pulse spectrometer by performing THz linear autocorrelation directly with the THz beam. To accomplish this we have addressed the two key issues. First, we implemented high-resistivity silicon as broadband and nearly lossless THz beam splitter. Second, Michelson interferometer mirrors are focusing and matching the acceptance angle of the Winston cone – the collection paraboloid in front of the liquid helium cooled bolometer.

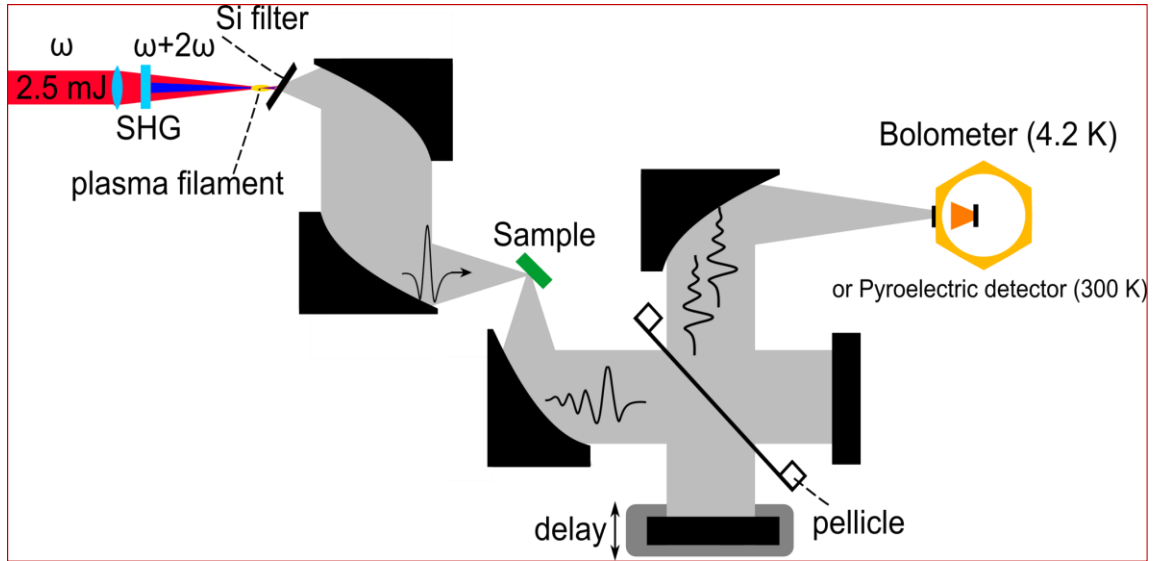


**Figure 4:** Schematic of a broadband THz spectrometer. As depicted, THz is generated via co-focusing fundamental ( $\omega$ ) and second harmonic (SHG,  $2\omega$ ) pulses into air generating plasma at the focus; generated THz is focused onto the sample and then sent into a Michelson interferometer for linear autocorrelation (detected by means of pyroelectric or bolometer (shown) detectors), where THz beam is split either by pellicle or a high resistivity Silicon filter (not shown). THz emission studies can be performed simply by exciting sample with the NIR pulses directly (not shown).

To study THz reflectance, we employ an established THz generating scheme [12,13]. A hybrid optical field is formed by the fundamental and second harmonic frequencies of an amplified ultrashort laser pulse, shaped with the proper relative phase delay. This hybrid pulse is focused to induce optical gas breakdown. The nonlinear interaction of the light with the plasma – still not well understood and the subject of some controversy -- produces a broadband, directional THz pulse. We showed (Figure 5, left) that the bandwidth of the generated pulse exceeds 20 THz, which is ideal for the measuring the far-infrared reflectivity spectra of our semiconductor devices. To verify adequate performance of our THz reflectance spectrometer, we performed calibration scans of bulk InAs reflectance (Figure 5, right) where we identify longitudinal bulk plasmon ( $\sim 2$  THz) as well as Coulomb-shifted longitudinal optical phonon ( $\sim 7.4$  THz). This is in great agreement with the theoretical fit (red line) [14].

A complimentary measurement to reflectance is to induce THz emission from the sample directly. Here, a single ultrashort laser pulse excites coherent plasmon and phonon macroscopic dipoles that can radiate into free-space and be detected. The laser pulses from our 1 kHz amplified system, however, are not suitable for such experiments because high peak intensity can cause permanent damage to semiconductor surfaces. Attenuating the beam to safe energy levels causes an unacceptable degradation of the signal-to-noise ratio. To address this problem, much lower energy pulses derived from a high repetition rate (89 MHz) broadband oscillator are used. We measure THz emission spectra by performing an autocorrelation of the emitted radiation, which is similar to an FTIR signal (Figure 4).

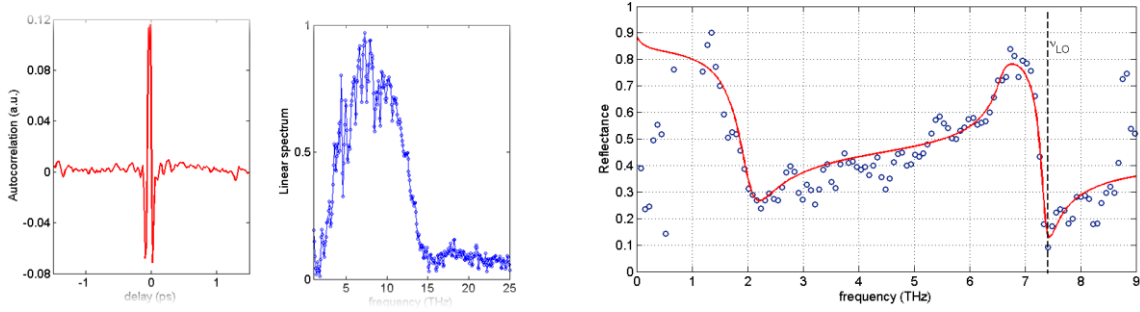


**Figure 5:** (left) THz autocorrelation and corresponding linear spectrum, as measured from the 2-color THz source: broadband emission exceeding 20 THz is observed; (b) proof-of-principle THz reflectance measurement of bulk InAs, clearly identifying plasmon ( $\sim 2$  THz) and Coulomb-shifted LO phonon ( $\sim 7.4$  THz) modes, which are in great a very good agreement with the theoretical curve (red line).

To excite high frequency collective modes (plasmons and phonons) of the samples, the exciting laser pulse duration must be substantially shorter than the characteristic oscillation period, which requires pulses shorter than  $\sim 25$  femtoseconds. For this purpose we implemented a pulse shaper/diagnostic unit (FemtoFit, Biophotonic Solutions). This device uses a spatial light modulator to impose a delay function on the spectral content of the pulse to control its spectral dispersion. An adaptive algorithm iteratively modifies this phase mask until it converges on a bandwidth-limited pulse duration. FemtoFit has produced pulses as short as 17 fs from our laser oscillator.

The numerical aperture of the THz detector (liquid helium cooled bolometer) is determined by its collection optics. This is a Winston cone, which is a contoured light pipe that focuses the incident radiation onto the detector element. We optimized the off-axis focusing geometry of the THz beam to match the numerical aperture of the bolometer, resulting in a factor of  $\sim 3$  improvement of the collection efficiency, as compared to a two-pulse THz spectrometer.

To demonstrate these improvements, we obtained THz emission of bulk InAs upon excitation with a short pulse (Figure 6). As expected (Figure 5), bulk plasmon ( $\sim 2$  THz) and longitudinal optical phonon ( $\sim 7.4$  THz) are clearly observed as peaks in the THz emission spectrum.

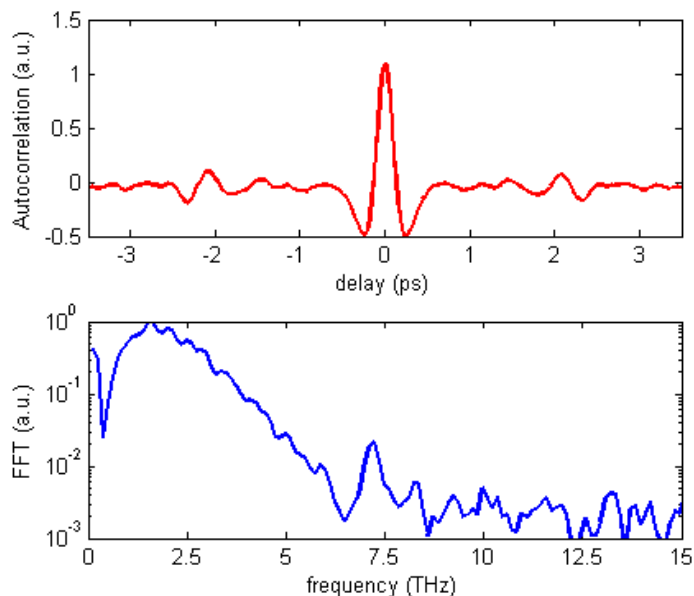
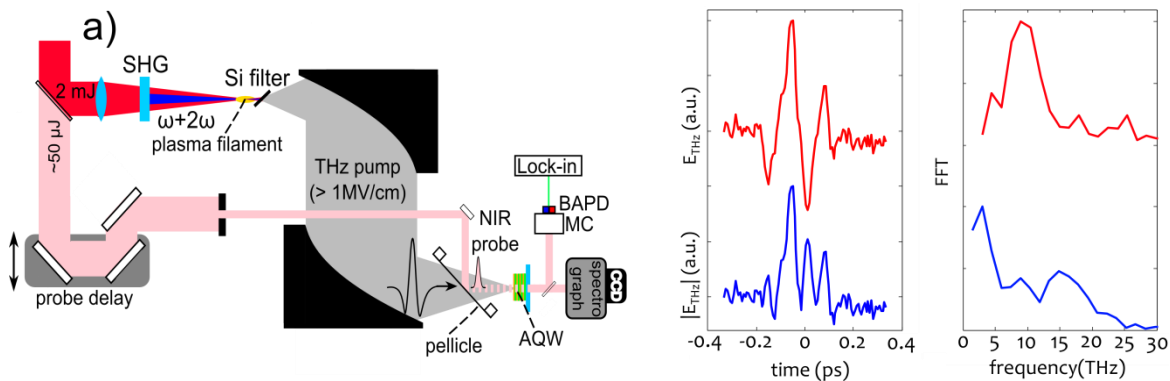


**Figure 6:** Autocorrelation trace (top) and a corresponding Fourier transform (bottom) of THz emission from a bulk InAs sample. A broad acoustic plasmon peak at  $\sim 2$  THz and emission from the bulk InAs LO phonon emission at  $\sim 7.4$  THz are clearly observed.

## b) Coherent detection

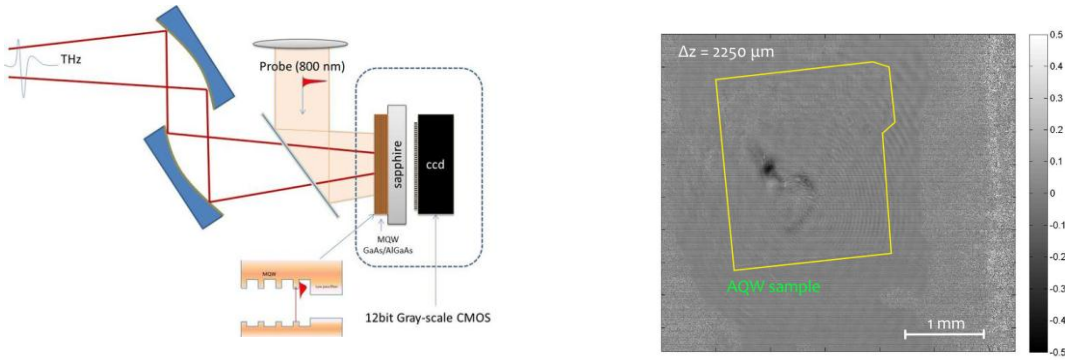
Broadband THz sensing has been performed by bolometric detection which requires liquid He. This is costly and relatively slow. On the other hand, coherent detection using conventional electro-optic sampling has offered a sensitive alternative but only for spectral range  $< 3$  THz. We have investigated THz electro-absorption modulation in semiconductor quantum wells as an alternative. The so-called electro-absorptive sampling is inherently very fast as it does not rely on phase matching conditions [15]. To this end, using our collaboration with SNL colleagues, we are investigating THz electro-absorption in GaAs/AlGaAs asymmetric double quantum wells (AQW) for coherent detection.

Figure 7 (left) depicts our modified experimental setup, where plasma THz generation technique discussed above is used to produce THz peak pump field of approximately 1 MV/cm. Spatial and temporal overlap of the THz pump and near-infrared probe is maintained on the AQW samples. The presence of THz pump modulates the interband absorption, resulting on delay-dependent transmission modulation, as can be measured by a monochromator/detector pair or by a CCD. Figure 7 (right) depicts normalized differential transmission of the probe beam at 833 nm, corresponding to below-bandgap absorption in the ADQW. Linear dependence of this signal on the square root of the THz power (not shown), allows us to interpret EA signal as an absolute value of the THz field, showing rectified behavior, characteristic of Franz-Keldysh below-gap absorption modulation. Therefore, we can also linearize the signal, yielding coherent THz signal with  $n\pi$  phase ambiguity [16].



**Figure 7:** (a) Schematic of a broadband (0.5-25 THz) THz pump and NIR probe electro-absorption (EA) sampling experiment; THz pump (1MV/cm) is combined with NIR probe at the asymmetric quantum well (AQW) sample; EA modulation of probe transmission at 833 nm (below AQDW bandgap), showing rectified field, characteristic of Franz-Keldysh response; linear power dependence (not shown) allows us to interpret EA signal as  $|E_{THz}|$  and hence coherent detection (red, top) with phase ambiguity of  $n\pi$ .

In addition to coherent detection, electro-absorption sampling (EAS) lends itself nicely to high contrast THz imaging using standard CCD (or CMOS) sensors as depicted in Fig 8.



**Figure 8:** (left) schematic of an EAS THz imaging system using standard CMOS sensors; (right) measured THz image (dark area) within the ADQW sample (yellow border).

Here, spatial EA modulation is registered by the probe beam and the probe area (sample) is imaged onto a VIS-NIR imager (CCD or CMOS camera). Figure 8 shows proof-of-principle demonstration of THz imaging based on EAS, where dark features highlight strong THz astigmatism at the focal plane of a high-NA parabolic off-axis mirror [16].

#### IV. THz reflection and emission studies of ordered nanowires.

One of the key observations in explanation of the THz emission mechanism in nanowires has been the invocation of the bulk plasmon at high frequency, which is  $\sim 12$  THz for our InAs NW samples. To test this, we employed broadband THz reflection spectrometer and the results are shown in Figure 9. Several features are observed in the presented data.

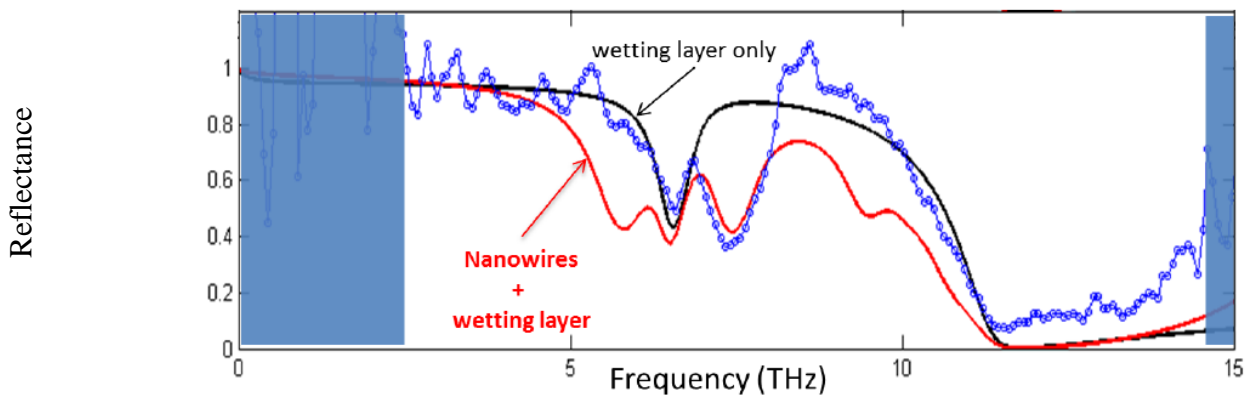


**Figure 9:** Measured reflectance spectrum of nanowire ensemble (blue) with several fits including wetting layer only (black), as well as nanowire + wetting layer (red). Clearly, the "wetting layer" case alone cannot reproduce all features of the observed spectrum, note the plasmon edge at 12 THz is observed, further supporting acoustic plasmon model.

First and foremost, plasmon dip at 12 THz is clearly resolved in good quantitative agreement with earlier prediction based on the acoustic-plasmon model [1]. Thus, this measurement offers further support of the picture of the acoustic-plasmon emission. Next observation can be made about the multiple dips observed in the reflection spectra between 5 and 10 THz [17]. To account for possible contributions of the wetting layer, we

attempted to fit the data with phonon-only peak ("wetting layer only" case, black line in Fig 9), which clearly does not reproduce all the features of the data. Using the full dielectric function of the NW, supplemented by the phonon contribution, we fit the data with equally-weighted functions of NW and wetting layer reflectance, shown in red curve. A better agreement is observed, qualitatively describing the features observed in the reflectance data in Fig 9 (areas with low signal-to-noise ratio are grayed out).

In addition to reflectance measurements, we have also studied emission properties of NW arrays and in particular from the spatially-ordered array of InAs nanowires (NWs), or microposts. These samples are grown by our collaborators at Sandia National Laboratories, Albuquerque NM. In this growth, NW length and geometry was varied using the novel fabrication technique, developed at SNL. Briefly, self-assembled polymer micro-spheres, arranged in a honeycomb lattice geometry, and pattern the surface of a bulk InAs substrate. Selective etch then removes substrate only in the areas, exposed in the voids between the spheres. By careful control of the etch process and sphere size, NWs of variable respective length and diameters can be obtained. Polymer spheres are removed in the final etch. In this study we interrogated emission from three samples of varying post height: 1  $\mu\text{m}$ , 2  $\mu\text{m}$  and 4  $\mu\text{m}$ . Length of the NWs posts was doubled each time to study the effect of spectral dependence of the NW emission on the NW aspect ratio, as predicted in theory. Shortest posts, namely 1  $\mu\text{m}$  have suffered from severe overetch of the top portions of the post, resulting in hexagonal pyramid geometry, Figure 10. These samples have proven to have most broadband THz emission, as presented below.

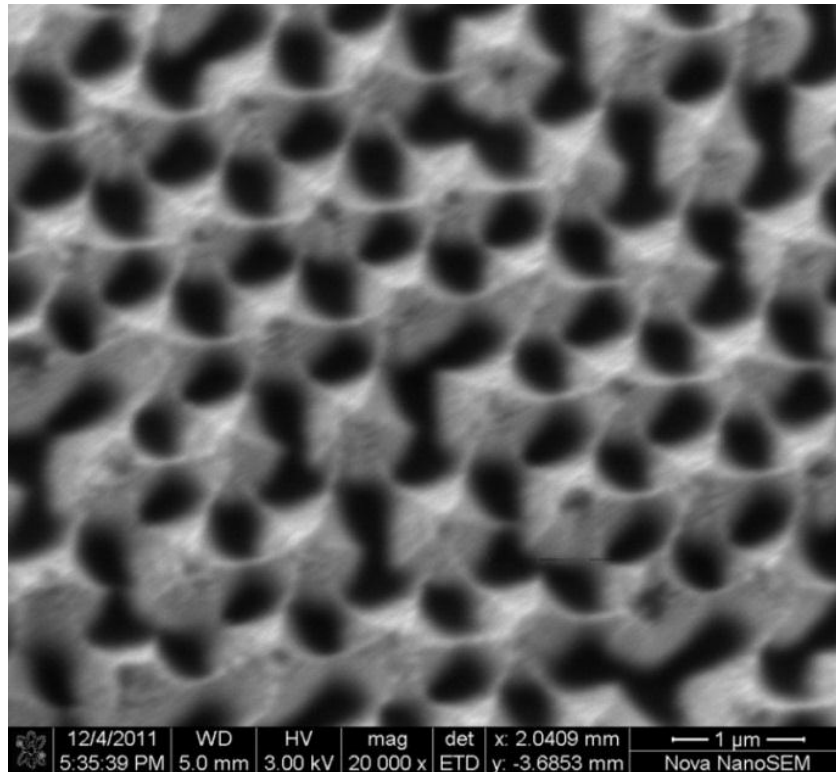


**Figure 10:** SEM image (top view) of the “pyramid” posts, resulting from over-etching of the top of the NW posts.

Emission of the three NW post samples is depicted in Figure 11. Top of the figure is showing THz emission spectrum of a 2  $\mu\text{m}$  height posts, middle: 4  $\mu\text{m}$  and bottom 1  $\mu\text{m}$  “pyramids” as a function of pump polarization ( $\sigma$  in blue and  $\pi$  in red).

It is clear that emission spectra consist from 3 contributions: a low-frequency ( $\sim 2$  THz) peak, followed by a secondary peak at  $\sim 4$  THz and finally weak emission at  $> 8$  THz. It should also be noted that 2 THz peak is

the most sensitive to the pump polarization. Thus, we attribute 2 THz peak to the bulk InAs emission, as it is consistent with a plasma frequency of a nominally-doped InAs substrate and is sensitive to the pump polarization, due to Fresnel losses of the pump light for  $\sigma$ -polarized light (blue traces in Figure 11). Coupling of the pump light to NW posts should be less sensitive to the pump polarization because of the curved surfaces of the latter, which tend to “mix” polarization components, i.e. even a purely  $\sigma$  or  $\pi$ -polarized pulse in a laboratory frame will have both  $\sigma$  and  $\pi$  components of the excitation with respect to the curved NW surface. Thus, spectral contribution at  $\sim 4$  THz of the overall emission signal is attributed to the NWs. Finally, the highest frequency  $\sim 8$  THz feature results from THz emission of the LO-phonon mode in the NWs. We can attribute this emission to NWs since frequency shift from the bare phonon at 7.3 THz is consistent with the coupled plasmon-phonon mode (plasmon mode in NW is attributed to the  $\sim 4$  THz feature).

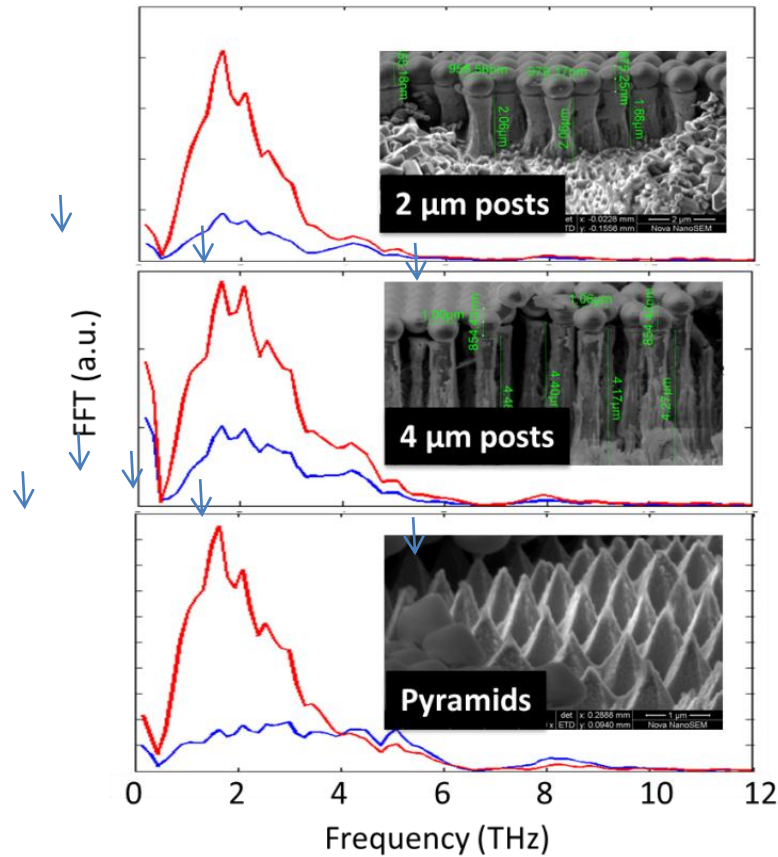


**Figure 11:** Fast Fourier transform (power spectra) of the NW THz emission. Emission from 2  $\mu\text{m}$  posts (top), 4  $\mu\text{m}$  posts (middle) and 1  $\mu\text{m}$  cones are shown as a function of  $s$ - (blue) and  $p$ - (red) polarized pump beam.

Upon closer inspection of the emission spectra from the 2  $\mu\text{m}$  and 4  $\mu\text{m}$  posts it is evident that in addition to the 2 THz and 4 THz peaks, 4  $\mu\text{m}$  posts also exhibit a peak around 3 THz. While these observations remain to be confirmed in additional experiments, if they hold true, this would be precisely consistent with the theoretical prediction of the plasmon eigen-frequency dependence in the NW geometry on the aspect ratio. More specifically, shorter NW will exhibit higher frequency cut-off of the lowest longitudinal acoustic plasmon frequencies. By comparing Figure 11 (top) and (middle) we argue that evidence for 2 and 4 THz peaks in the former, combined with a possible presence of 1, 2, 3, 4 THz peaks in the latter cases argues for observation of the acoustic surface plasmon contribution to the THz emission, as we have shown previously for the disordered NWs. Finally we note that the case of “pyramids” exhibits a very interesting spectrum, almost featureless and extremely broadband, covering up to 9 THz, with a shallow dip at  $\sim 7$  THz. While we are in the process of modeling THz emission from conical plasmon cavities, we can apply general arguments that the “pyramid”

shape results from a superposition of continually-varying aspect-ratio of the cylindrical cavities. Thus, THz emission from such superimposed NWs will result in broadening of the features. Also, shorter NWs at both high and low aspect ratios, would explain  $> 4$  THz and  $< 2$  THz frequency components, broadening emission, as qualitatively compared to the cylindrical cavities (top and middle panels of Figure 3). We also note that observed blue-shift is further accompanied by a strong shift of the phonon-like mode of the hybrid plasmon-phonon system at 9 THz, consistent with model predictions and our previous experimental work on highly-doped InAs substrates.

Thus, our first results suggest a possibility to control low-frequency acoustic surface plasmon modes in these NWs by variation of the NW aspect ratio. An extremely broadband emission from “pyramids” might suggest applications for a broadband THz source.

## **V. Dissemination of this work**

This work has been widely disseminated by presentations at various international conference meetings, proceedings and peer-reviewed publication. A total of 8 presentations (including Ref. 16 and 1 invited talk), written conference proceedings (Proceedings of SPIE, total of 3, including Ref 15,17) and peer-reviewed journal publication (Ref 1). The latter has been chosen as “Editor’s Suggestion” by the Editorial board of the Physical Review B journal (September 2011 issue) and was featured in “Research Highlights” section of the Nature Photonics journal in the November 2011 issue [18], the reproduction of which can be viewed in Appendix A.

## **VI. Conclusions**

In this work we have performed detailed experimental investigation of THz emission mechanisms in InAs nanowires. Three independent experiments of THz emission, THz reflection and DC transconductance measurements are brought into quantitative agreement by means of a model which includes contributions of quantized surface plasmon modes of the cylindrical geometry of the nanowire. It is inferred from the model that low-energy acoustic surface plasmon modes are the dominating contributors to the THz radiation, observed following ultrafast excitation of this material system. While our results were obtained for InAs nanowires, we believe that our conclusions do apply in general to any nanoscale emitters, described within the framework of our model. In addition, enhanced emission from the nanowires was observed, proving them as potential candidates for applications where high efficiency nanoscale THz emitters are desired, such as for example imaging of electronic properties of modern photonic devices on the nanoscale.

In parallel efforts, we have also investigated THz emission from ordered array of InAs nanowires. This has led us to development of novel fabrication method of nanopost arrays, including hexagonal “pyramid” structure. The latter has proven as extremely broadband (octave-spanning) THz nanoscale emitter source which can also be attractive for a variety of applications. In performing THz emission studies of InAs nanowires we have for the first time observed THz emission from coherently excited phonon modes in the wires. Average size of the nanowires does not lead to modification of phonon dispersion at room temperature, however phonon quantization might be revealed at low temperatures, -- an intriguing subject for future the future studies.

The results presented here were possible by implementation of improved and novel THz detection schemes. A conventional THz spectrometer has been modified to provide broadband operation exceeding 20 THz. In addition, novel electro-absorption sampling technique has been developed utilizing multiple quantum well structures. Franz-Keldysh effect has been identified as the main detection mechanism and we have shown that

coherent detection of THz pulse is possible for electro-absorption signal probed below the band-gap of the multiple quantum well detector. We have also demonstrated THz imaging with electro-absorption effect using conventional (visible wavelengths) imaging systems.

## References:

- [1] D.V. Seletskiy, M.P. Hasselbeck, J.G. Cederberg, A. Katzenmeyer, M.E. Toimil-Molares, F. Léonard, A.A. Talin, M. Sheik-Bahae, “Efficient terahertz emission from InAs nanowires”, *Phys. Rev. B* **84**, 115421 (2011).
- [2] J. Pendry, *Science* **285**, 1687 (1999).
- [3] H. A. Atwater, *Sci. Am.* **296**, 56 (2007).
- [4] K. Wang and D. M. Mittleman, *Nature* **432**, 376 (2004).
- [5] T.W. Ebbesen, H. J. Lezec, H. F. Ghaemi, T. Thio, and P. A. Wolff, *Nature* **391**, 667 (1998).
- [6] A. J. Huber, F. Keilmann, J. Wittborn, J. Aizpurua, and R. Hillenbrand, *Nano Lett.* **8**, 3766 (2008).
- [7] R. P. Prasankumar, P. C. Upadhyaya, and A. J. Taylor, *Phys. Status Solidi B* **246**, 1973 (2009).
- [8] A. A. Talin, F. Leonard, A. M. Katzenmeyer, B. S. Swartzentruber, S. T. Picraux, M. E. Toimil-Molares, J. G. Cederberg, X. Wang, S. D. Hersee, and A. Rishinaramangalum, *Semicond. Sci. Technol.* **25**, 024015 (2010).
- [9] J. M. Pitarke, J. B. Pendry, and P. M. Echenique, *Phys. Rev. B* **55**, 9550 (1997).
- [10] D. Seletskiy, Ultrafast Terahertz Spectroscopy and Control of Collective Modes in Semiconductors, Ph.D. Thesis, University of New Mexico, Albuquerque, NM, USA, 2010.
- [11] R. Kersting, J. N. Heyman, G. Strasser, and K. Unterrainer, *Phys. Rev. B* **58**, 4553 (1998).
- [12] D. J. Cook and R. M. Hochstrasser, *Opt. Lett.* **25**, 1210-1212 (2000).
- [13] Xu Xie, Jianming Dai, and X.-C. Zhang, *Phys. Rev. Lett.* **96**, 075005 (2006).
- [14] C. Kittel “Introduction to Solid State Physics” 7<sup>th</sup> edition, Wiley (1995).
- [15] C.-Y. Li, D.V. Seletskiy, J.G. Cederberg, M. Sheik-Bahae, “Detection of ultrafast THz pulses via electro-absorption in coupled asymmetric quantum wells”, *Photonics West* (San Francisco, Jan 21-26, 2012), paper **8260-21**.
- [16] C.-Y. Li, D. V. Seletskiy, J. Cederberg, M. Sheik-Bahae, “Quantum-Well Electro-Absorption Sampling for Broadband THz Detection”, *CLEO* (San Jose, May 6-11, 2012), paper **QTu1H.8**.
- [17] D.V. Seletskiy, C.-Y. Li, J.G. Cederberg, A. Katzenmeyer, E. Morales, F. Leonard, A. Talin, M. Sheik-Bahae, “Strong THz emission from low-energy acoustic-like surface plasmons in InAs nanowires”, *Photonics West* (San Francisco, Jan 21-26, 2012), paper **8260-12**.
- [18] N. Horiuchi "Nanowire emitters" *Nature Photonics* **5**, 712–713 (2011).

**Appendix A:** Research highlight of our work by Nature Photonics, written for broad audience.



**research highlights**

D. V. Seletskiy, M. P. Hasselbeck, J. G. Cederberg, A. Katzenmeyer, M. E. Toimil-Molares, F. Leonard, A. A. Talin, A. and M. Sheik-Bahae, "Efficient terahertz emission from InAs nanowires," Phys. Rev. B 84, 115421 (2011) [This paper was selected for PRB's Editors' Selection].

## Nanowire emitters

*Phys. Rev. B* **84**, 115421 (2011)

Nanoscale emitters of terahertz radiation would be useful for a variety of applications, including investigations into the physical properties of nanostructured materials. Denis Seletskiy and co-workers of the University of New Mexico, Sandia National Laboratories and Air Force Research Laboratory in the USA have now shown that InAs nanowires may be suitable nanoscale sources of terahertz radiation. The researchers first prepared gold nanoparticles as InAs growth precursors on the GaAs substrate surface and then used metal-organic vapour phase epitaxy to fabricate InAs nanowires perpendicular to the substrate. The nanowires were 10–20  $\mu\text{m}$  tall and had diameters that tapered from 450 nm at the base to 60 nm at the tip. Terahertz wave generation was achieved by illuminating the nanowires at an incident angle of  $45^\circ$  with 820 nm, 60 fs pulses from a Ti:sapphire laser. The researchers measured spectra of up to 5 THz through a linear autocorrelation technique. Taking into account the fact that the filling factor of the nanowires was only around 0.03, the radiation power was about

15 times larger than that of a bare planar InAs substrate. The researchers suggest that the presence of a low-energy acoustic surface plasmon mode was responsible for terahertz emission.

NH

**DISTRIBUTION LIST  
DTRA-TR-13-64**

**DEPARTMENT OF DEFENSE**

DEFENSE THREAT REDUCTION  
AGENCY  
8725 JOHN J. KINGMAN ROAD  
STOP 6201  
FORT BELVOIR ,VA 22060  
ATTN: J. REED

DEFENSE TECHNICAL  
INFORMATION CENTER  
8725 JOHN J. KINGMAN ROAD,  
SUITE 0944  
FT. BELVOIR, VA 22060-6201  
ATTN: DTIC/OCA

**DEPARTMENT OF DEFENSE  
CONTRACTORS**

EXELIS, INC.  
1680 TEXAS STREET, SE  
KIRTLAND AFB, NM 87117-5669  
ATTN: DTRIAC